TECHNICAL ARTICLE

Total scattering experiments on glass and crystalline materials at the ESRF on the ID11 Beamline

Andrea Bernasconi,[a] Jonathan Wright, and Nicholas Harker
ESRF – The European Synchrotron – Grenoble, France

(Received 29 September 2014; accepted 17 November 2014)

ID11 is a multi-purpose high-energy beamline at the European Synchrotron Radiation Facility (ESRF). Owing to the high-energy X-ray source (up to 140 keV) and flexible, high-precision sample mounting which allows small sample–detector distances to be achieved, experiments such as total scattering in transmission geometry are possible. This permits the exploration of a wide Q range and so provides high real-space resolution. A range of samples (glasses and crystalline powders) have been measured at 78 keV, first putting the detector as close as possible to the sample (~10 cm), and then moving it vertically and laterally with respect to the beam in order to have circular and quarter circle sections of diffraction rings, with consequent Q_{MAX} at the edge of the detector of about 16 and 28 Å^{-1}, respectively. Data were integrated using FIT2D, and then normalized and corrected with PDFgetX3. Results have been compared to see the effects of Q-range and counting statistics on the atomic pair distribution functions of the different samples. A Q of at least 20 Å^{-1} was essential to have sufficient real-space resolution for both type of samples while statistics appeared more important for glass samples rather than for crystalline samples. © *2014 International Centre for Diffraction Data.* [doi:10.1017/S0885715614001304]

Key words: PDF, synchrotron, glass, crystalline

I. INTRODUCTION

Scientific interest in performing total scattering experiments (Bragg and diffuse scattering) is increasing, owing to the ability of this technique to unravel the disordered structure in crystalline phases as well as in glasses and liquids. For this reason, scientists are continuously looking toward improvements in data quality, both at large-scale synchrotron facilities and from conventional laboratory instruments, and also on the data reduction, which is quite delicate for these kinds of experiments.

Regarding data quality, high scattering angles and/or high-energy radiation are required to explore a wide momentum transfer (Q) range ($Q = 4\pi\sin\theta/\lambda$). This needs to be combined with good statistics, especially at high Q where the diffuse scattering is dominant and the data are most sensitive to small atomic shifts. For proper background subtraction and normalization, the data need to be acquired with a stable incident beam (Billinge, 2009).

At synchrotron radiation facilities, one common way to satisfy these requirements is to perform the experiment in transmission geometry, with the data collected using a two-dimensional (2D) detector; this setup allows also fast data acquisition that is particularly suitable when time resolution is required (Ponchut, 2006).

As for crystallographic experiments, pair distribution function (PDF) analysis requires the sample–detector parameter calibration, azimuthal integration, and incident angle corrections (Wu *et al.*, 2002), in order to extract the 1D scattering intensity $I(Q)$ from the 2D image. Afterwards, to extract information from deviations in the periodic atomic arrangement, coherent intensity I_C is extracted from the measured intensity I_M, following equation (Juhas *et al.*, 2013):

$$I_M(Q) = a(Q)I_C(Q) + b(Q), \tag{1}$$

where $a(Q)$ and $b(Q)$ are multiplicative and additive corrections like self-absorption and X-ray polarization, and Compton and container scattering, respectively. The I_C function, which includes both Bragg and diffuse scattering, is then normalized for the scattering factors (atomic form factors for X-rays which are Q-dependent; and scattering length b for neutrons which are independent of Q). This gives the total scattering function $S(Q)$, as shown in the equation:

$$S(Q) = \frac{\left(I_C(Q) - f(Q)^2 + f(Q)^2\right)}{f(Q)^2}. \tag{2}$$

This $S(Q)$ function is sine Fourier transformed to obtain $G(r)$, defined as the pair distribution function, following the equation:

$$G(r) = \left(\frac{2}{\pi}\right)\int_{Q_{min}}^{Q_{max}} Q[S(Q) - 1]\sin Qr\, dQ. \tag{3}$$

This contains the real-space information which reveals the local structure of the investigated sample and also information about grain size from $G(r)$ from amplitudes at high r, that are particularly important for nanomaterials (Masadeh *et al.*, 2007).

[a]Author to whom correspondence should be addressed. Electronic mail: andrea.bernasconi@esrf.fr

TABLE I. Molar composition (expressed as oxide fractions) of the two investigated glass samples.

Sample	SiO_2	Al_2O_3	Na_2O	ZnO
A	0.76	0.076	0.14	0.024
B	0.68	0.068	0.14	0.112

The present paper is aimed at evaluating some effects of the processed data range (e.g. Q_{MAX}) and of the acquisition statistics (e.g. azimuthal integration range) on the $G(r)$ of some glassy and crystalline materials.

The experiments have been performed at the Material Science ID11 beamline [European Synchrotron Radiation Facility (ESRF)] that is particularly suitable for total scattering experiments because of its high-energy source (18–140 keV), combined with a transmission geometry and a fast 2D charge coupled device (CCD) area detector (Frelon camera, Labiche *et al.*, 2007).

II. EXPERIMENTAL METHODS

A. Sample

Si NIST SRM640c was used to perform the initial calibration before a range of crystalline and glass materials were investigated. The crystalline samples were nanocrystalline CeO_2 and an industrial grade ZnO, whose mineralogical purity have been checked by matching with CeO_2 and ZnO *d*-spacings from Wyckoff (1963) and Xu and Ching (1993), respectively.

The glassy materials were two aluminosilicate glasses with different amount of zinc which had been prepared by quenching from 1200 °C and ground in a zirconia mortar; their molar compositions are summarized in Table I.

The powders were loaded in kapton capillaries with internal diameter of 1.5 mm.

B. Data collection

Measurements were performed in transmission geometry at the ID11 experimental hutch 1 with a 2D Frelon camera. Energy calibration was performed on Si NIST SRM640c material, following the method of Hong *et al.* (2012) at seven different sample–detector distances.

All data were collected with the detector as close as possible to the sample (distance ∼10 cm) and then moving it laterally and vertically with respect to the beam in order to have circular and quarter of circle sections of diffraction rings, as shown in Figure 1. Consequently, the Q_{MAX} at the edge of the detector was 16 and 28 $Å^{-1}$, respectively. The maximum achievable theta angle equals [arctan(*D*/*R*)]/2, where *D* is the sample–detector distance and *R* is the radius of the inscribed circle in the 2D-detector. However, if the radius of the circumscribed circle is considered, then a higher Q_{MAX} can be obtained in both configurations (e.g. 22 and 36 $Å^{-1}$, respectively), with the drawback that the azimuthal integration is limited only to the image diagonal. Thus, a larger range Q_{MAX} is available from the image corners, but these data are not available at all azimuthal angles, which may eventually cause problems to properly account for factors such as polarization, etc.

To increase the statistics, 20 images per samples were collected, with an exposure time that was 5 and 20 s for crystalline and glass samples, respectively.

C. Data reduction

The 2D images need to be integrated to obtain intensity as function of 2θ, or Q, or *d*-spacing, which was done using the FIT2D program (Hammersley *et al.*, 1996). This reduction method needed (i) dark current images with the same exposure time to subtract from the raw image to remove the electronic signal not generated by X-ray radiation; (ii) flood image from the detector that describes the different response of each detector pixel to X-ray radiation; and (iii) the spatial distortion of the detector.

Afterwards, because of the high energy of our measurements, the absorption of the X-ray beam in the phosphor may be less than 100% ("thin phosphor regime"), with a consequent detector response that depends on the incident angle α and the effective thickness of the phosphor. For this reason, following Wu *et al.* (2002), observed intensity I_{OBS} have been corrected using a phosphor contribution, expressed as $(1 - T_{\perp}^{phosphor})/\{1\text{-}\exp[\ln(T_{\perp}^{phosphor})/\cos(\alpha)]\}$, that considers α and phosphor transmission at a perpendicular incidence condition ($T^{phosphor}$). For completeness, we also considered the absorption contribution that comes from the protective faceplate in front of the phosphor that plays an opposite role, attenuating more of the signal at high α than at low α. The contribution from this faceplate, can be expressed as $T^{faceplate}/\{\exp[\ln(T^{faceplate}/\cos(\alpha)]\}$, where $T^{faceplate}$ is the faceplate transmission at the perpendicular incidence

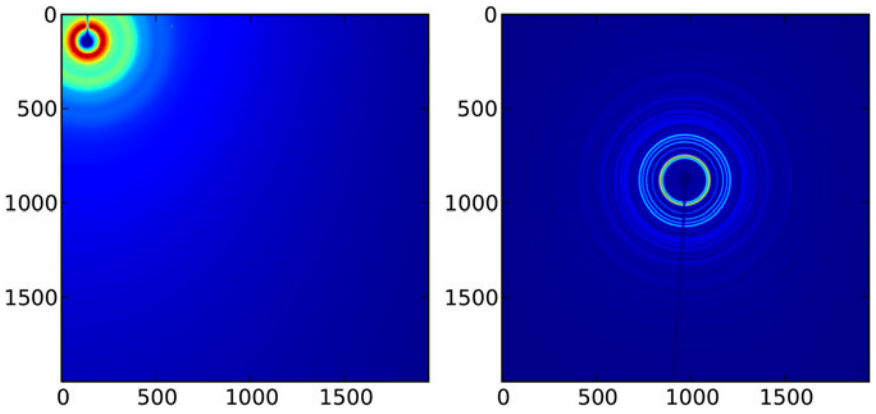

Figure 1. (Colour online) Examples of 2D images collected with the beam in the CCD corner on sample A (left side) and with the beam in the CCD center on ZnO sample (right side).

https://doi.org/10.1017/S0885715614001304 Published online by Cambridge University Press

condition. Therefore, the adopted equation to obtain the equivalent perpendicular-incidence intensity I from I_{OBS} using the Frelon camera is:

$$I_{\perp} = \frac{I_{OBS}\left(1 - T_{\perp}^{phosphor}\right)}{\left(1 - e^{\left(\ln\left(T_{\perp}^{phosphor}\right)/\cos\alpha\right)}\right)} \times \frac{T_{\perp}^{faceplate}}{\left(e^{\left(\ln\left(T_{\perp}^{faceplate}\right)/\cos\alpha\right)}\right)}. \quad (4)$$

$T_{\perp}^{faceplate}$ and $T_{\perp}^{phosphor}$ were directly measured at the ID11 beamline at the energy of 78 keV. The $T_{\perp}^{faceplate}$ term changes when an absorbing screen is deliberately placed in front of the detector in order to reduce the background because of X-ray florescence (lower-energy X-rays are preferentially absorbed).

Figure 2 is an example of sample A raw data without (red curve) and with (black curve) the application of Eq. (4). For this sample, at a Q-value of 25 Å^{-1}, I_{OBS} would be overestimated by up to 8.3% without the application of Eq. (4). Moreover, the effect of the two distinct correction terms is also plotted, showing that at the energy of 78 keV the contribution of the phosphor is dominant with respect to the contribution from the faceplate.

Finally, the data (with correction for incident angle) were processed with PDFgetX3 (Juhas *et al.*, 2013), one of the most common total scattering pair distribution programs to obtain $S(Q)$ and $G(r)$, in agreement with Eqs (1)–(3).

III. RESULTS AND DISCUSSION

Energy calibration using Si NIST SRM640c as reference material, provided a wavelength coming from the double bent laue ID11 monochromator of 0.158 636(50) Å and a sample detector distance of 97.018 mm.

The resolution of the present experimental setup was estimated by looking at the evolution of Si peaks full-width at half-maximum (FWHM) as function of Q, as displayed in Figure 3.

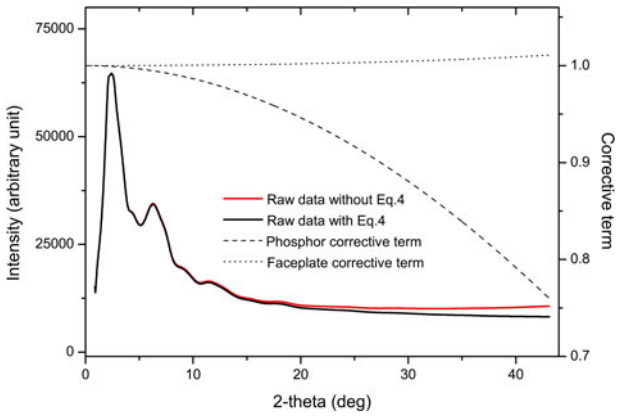

Figure 2. (Colour online) Sample A raw data without (red line) and with (black line) the application of incident angle correction using Eq. (4). Effects of phosphor and faceplate corrective terms of Eq. (4) are also plotted as dashed and dotted lines, respectively.

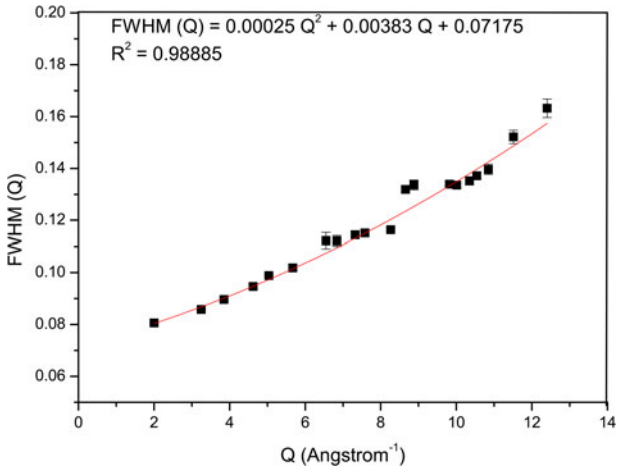

Figure 3. (Colour online) Instrumental resolution obtained by Pseudo-Voigt fit (used in 0–8 Å^{-1} range) and Gaussian fit (used in 8–13 Å^{-1} range) of Si NIST SRM640c peaks at different Q-values (beam was in the CCD corner). For each selected peak, the R^2 of the Pseudo-Voigt/Gaussian fit to determine FWHM was always above the values of 0.99. Afterwards, 20 different points have been fitted with a 2nd degree polynomial function (red line).

In order to evaluate the role of Q range and statistics on the resultant $G(r)$, different integration ranges were selected when using the FIT2D program, summarized in Table II.

When reducing the azimuthal range from 90° to 20° to increase the Q_{MAX}, the polarization effect may be an issue that needs to be taken into account and corrected (Kahn and Fourme, 1982); however, in the present work, if differently oriented slices of 20° are selected when doing the azimuthal integration, the resultant crystalline and glass $G(r)$s did not exhibit significant differences after processing with FIT2D and PDFgetX3.

Applying Eq. (4) influences the peak amplitudes in $G(r)$, increasing peak heights as displayed in Figure 4.

A. Crystalline samples

For the crystalline samples, both nanocrystalline CeO_2 and industrial grade ZnO were used to evaluate the effect of Q range and the role of counting statistics. These data were processed with PDFgetX3, using an r_{poly} values of 1.3 Å for CeO_2 and 1.2 Å for ZnO. These values were selected from a graphical inspection of $G(r)$.

In Figure 5, the $S(Q)$ for CeO_2 is shown (data collected with the beam center in the corner of the detector), along with a plot of the resultant $G(r)$s as function of different Q_{MAX} values. The different real-space resolution (mainly function of π/Q_{MAX}) is displayed with the higher Q_{MAX} (i.e. 28 Å^{-1}, black line) by sharper peaks and truncations that are more frequent but lower in amplitude. This effect has been determined for both CeO_2 and ZnO, in terms of FWHM, by fitting with a Gaussian to the first metal–metal peaks in $G(r)$, which are the peaks with the higher amplitude. The results are summarized in Table III.

When refining these different patterns with popular software such as PDFGUI (Farrow *et al.*, 2009), after previous tuning of resolution parameters (i.e. Q_{DAMP} and Q_{BROAD}) a good agreement between the refined metal and oxygen U_{ISO} parameters has been observed, as a function of the different

https://doi.org/10.1017/S0885715614001304 Published online by Cambridge University Press

TABLE II. Integration strategy adopted for evaluate Q_{MAX} role (upper part) and statistic role (lower part) during processing with FIT2D.

Q_{MAX} role		
Type of image	Azimuthal range (deg)	Q_{MAX} from outer radius (Å^{-1})
Beam in the CCD center (Figure 1, right)	0–360	16
Beam in the CCD corner (Figure 1, left)	0–90	20
Beam in the CCD corner (Figure 1, left)	0–90	24
Beam in the CCD corner (Figure 1, left)	0–90	28
Statistic role		
Type of image	Azimuthal range (deg)	Q_{MAX} from outer radius (Å^{-1})
Beam in the CCD corner (Figure 1, left)	0–90	28
Beam in the CCD corner (Figure 1, left)	0–20	28

Qranges. However, when Q_{MAX} of 16 Å^{-1} is used, oxygen U_{ISO} was systematically and clearly bigger (as displayed in Table III).

The explanation for the U^{ISO} problem is the limited real-space resolution of the configuration with Q_{MAX} of 16 Å^{-1}, which drives the fit to a smearing of some peaks. As example, we refer to ceria $G(r)$ where, in the 9–10 Å range, one can observe a Ce–Ce peak at about 9.35 Å and a Ce–O peak at about 9.65 Å with a Q_{MAX} of at least 20 Å^{-1}, whereas only the Ce–Ce peak is present if Q_{MAX} of 16 Å^{-1} is used (see Figure 6).

As far as the effect of statistics on the resultant $G(r)$, FWHM of the peaks does not vary significantly if 90° or 20° of azimuthal integration range are used (Q_{MAX} was fixed at 28 Å^{-1}) and also the refined values of metal and oxygen U_{ISO} parameters are almost unchanged, as showed in Table III.

Because of that, the idea of increased Q range at the expense statistics looks reasonable: in fact, this may allow a better real-space resolution (0.098 Å instead of 0.112 Å), but it may induce less well-resolved signal and noise in the $S(Q)$. Therefore, PDFGUI Q_{DAMP} parameter, which describes PDF Gaussian envelope because of the limited Q-resolution, has been refined on Si NIST SRM640c, giving values of 0.0593 (33) for a Q_{MAX} of 32 Å^{-1} and azimuthal range of 20°, and 0.0599 (28) for a Q_{MAX} of 28 Å^{-1} and azimuthal range of 90°. As for the non-systematic peak broadening induced by noise at high Q, the PDFGUI Q_{BROAD} parameter resulted 0.0602 (59) in the case of Q_{MAX} of 32 Å^{-1} and azimuthal range of 20°, and 0.0607 (51) for a Q_{MAX} of 28 Å^{-1} and azimuthal range of 90°. Agreement is also present in terms of refined metal and oxygen U_{ISO} parameter, for CeO_2 and for ZnO, as summarized in Table III.

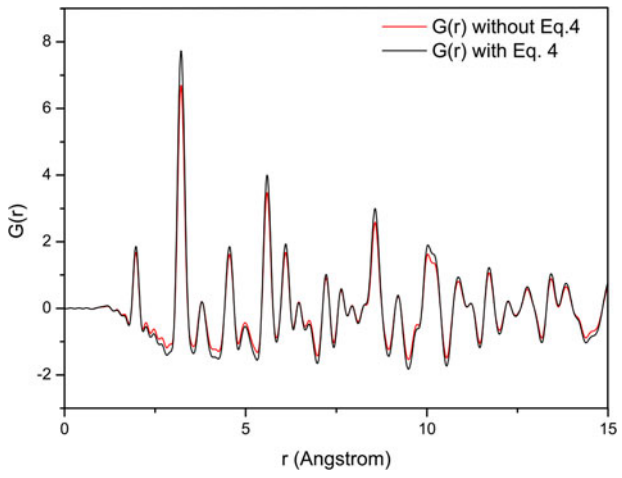

Figure 4. (Colour online) Zincite $G(r)$s without (red line) and with (black line) the application of incident angle correction using Eq. (4). Curves have been obtained with a Q_{MAX} of 28 Å^{-1} and an azimuthal range of 90°.

These considerations are important when dealing with some common problems in PDF data collection. For example, sample environments (e.g. systems for temperature control such as ovens, cryostream, heat blowers, etc.) can cause shadowing on regions of the detector for large scattering angles. Evidence here suggests that a reduced azimuthal range does not affect the quality of the $G(r)$.

From these samples and this experimental setup it is shown that a better real-space resolution can be achieved by reducing azimuthal range to increase Q_{MAX}, without affecting the statistics. Moreover, the configuration with the beam in the center of CCD is not recommended, because of its limited Q_{MAX}.

B. Glass samples

The diffraction pattern of amorphous materials is completely dominated by diffuse scattering, making the role of counting statistics crucial to minimize truncations during Fourier transform. On the other hand, Q_{MAX} is relevant when looking to resolve distances in complex compositions, as larger Q_{MAX} improves the real-space resolution.

This is the case for the two investigated aluminosilicate glasses: they differ in zinc content (see Table I) and have been compared following the same criteria as for the crystalline samples, as expressed in Table II, using PDFgetX3 program to process the data.

For these kinds of glasses, the Zn–O distance should be located at about 1.95 Å (Cassingham *et al.*, 2011). This was confirmed by some preliminary EXAFS measurements performed at BM23 beamline (ESRF).

As shown in Figure 7, Q range strongly affects Zn–O peak positions: there is a large error if Q_{MAX} of 16 Å^{-1} is used (black line), while it is close to the expected values (i.e. 1.95 Å) in the other cases. This is because of the better real-space resolution provided by a higher Q_{MAX}, especially when it is 28 Å^{-1} (blue line). A similar effect is also present

https://doi.org/10.1017/S0885715614001304 Published online by Cambridge University Press

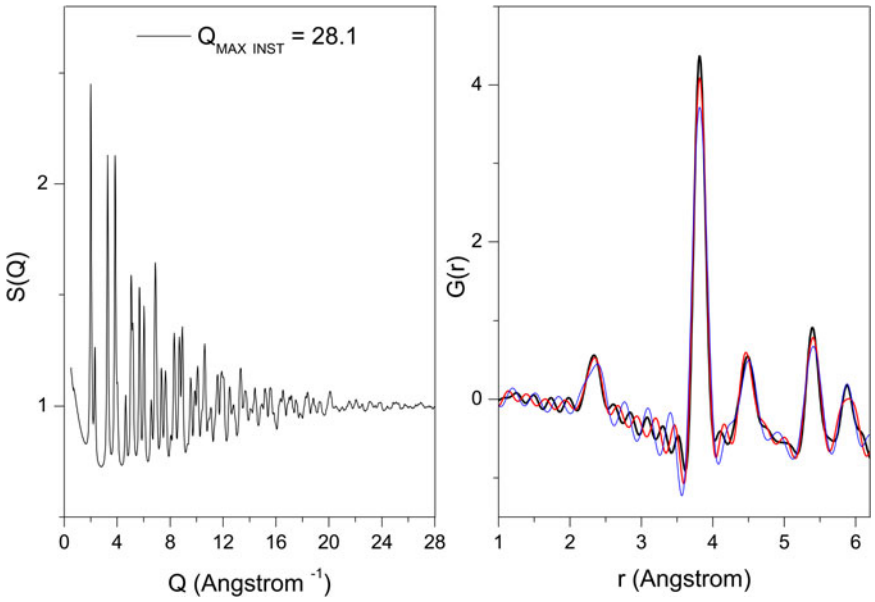

Figure 5. (Colour online) Total scattering $F(Q)$ function of nanocrystalline CeO_2, using an azimuthal integration range of 90° and Q_{MAX} of 28 $Å^{-1}$, on the left side. Comparison of $G(r)$ resulting from Fourier transform of the same $F(Q)$ but changing the Q_{MAX} from 28 $Å^{-1}$ (black line), 24 $Å^{-1}$ (red line), and 20 $Å^{-1}$ (blue line).

TABLE III. Full-width half-maximum (FWHM) of the first metal–metal peak in $G(r)$ and refined metal and oxygen U_{ISO} parameter in nanocrystalline CeO_2 and industrial grade ZnO, as function of Q_{MAX} and azimuthal range. Moreover, the R_W values from the PDFGUI fit are summarized. Fits have been performed in the 0.5–30 Å range.

		Nanocrystalline CeO_2				Industrial grade ZnO			
Q_{MAX}($Å^{-1}$)	Azimuthal range (deg)	FWHM M–M (Å)	Cerium U_{ISO} ($Å^2$)	Oxygen U_{ISO} ($Å^2$)	R_W (%)	FWHM M–M (Å)	Zinc U_{ISO} ($Å^2$)	Oxygen U_{ISO} ($Å^2$)	R_W (%)
16	90	0.3052 (33)	0.0024 (2)	0.0138(9)	15.54	0.3087 (31)	0.0038 (2)	0.0086(8)	14.87
20	90	0.2095 (40)	0.0024 (2)	0.0119(20)	16.96	0.2322 (18)	0.0038 (2)	0.0072(10)	18.63
24	90	0.1833 (29)	0.0024 (2)	0.0115(19)	17.95	0.2233 (16)	0.0037 (2)	0.0067(9)	19.15
28	90	0.1706 (29)	0.0025 (2)	0.0113(20)	18.45	0.2195 (13)	0.0038 (2)	0.0067(9)	19.28
28	20	0.1701 (32)	0.0025 (2)	0.0114(18)	18.59	0.2208 (14)	0.0038 (2)	0.0066(8)	19.42
32	20	0.1647 (31)	0.0023 (1)	0.0115(24)	18.98	0.2200 (10)	0.0038 (2)	0.0065(10)	19.56

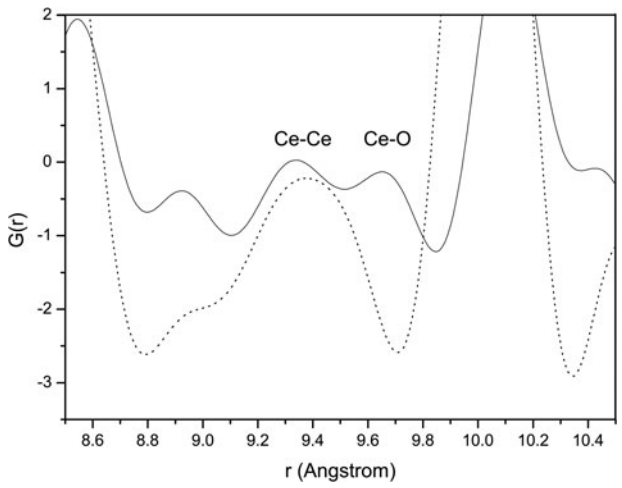

Figure 6. $G(r)$ magnification if Q_{MAX} of 20 $Å^{-1}$ (black line) and 16 $Å^{-1}$ (dashed line) are used. Owing to the different real-space resolution, the former is able to show both Ce–Ce and Ce–O peaks, located at about 9.35 and 9.65 Å, respectively, whereas the latter is able to show only the Ce–Ce peak.

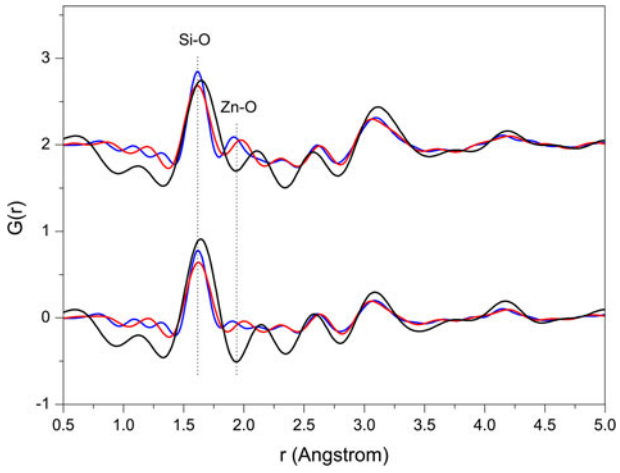

Figure 7. (Colour online) Samples A and B $G(r)$s as function of different adopted Q_{MAX}, obtained with PDFGetX3 program. Black curve is obtained with Q_{MAX} of 16 $Å^{-1}$, putting the beam in the CCD center, while blue and red curves have been obtained by putting the beam in the CCD corner, using an azimuthal range of 90° and a Q_{MAX} of 28 (blue line) and 20 $Å^{-1}$ (red line).

https://doi.org/10.1017/S0885715614001304 Published online by Cambridge University Press

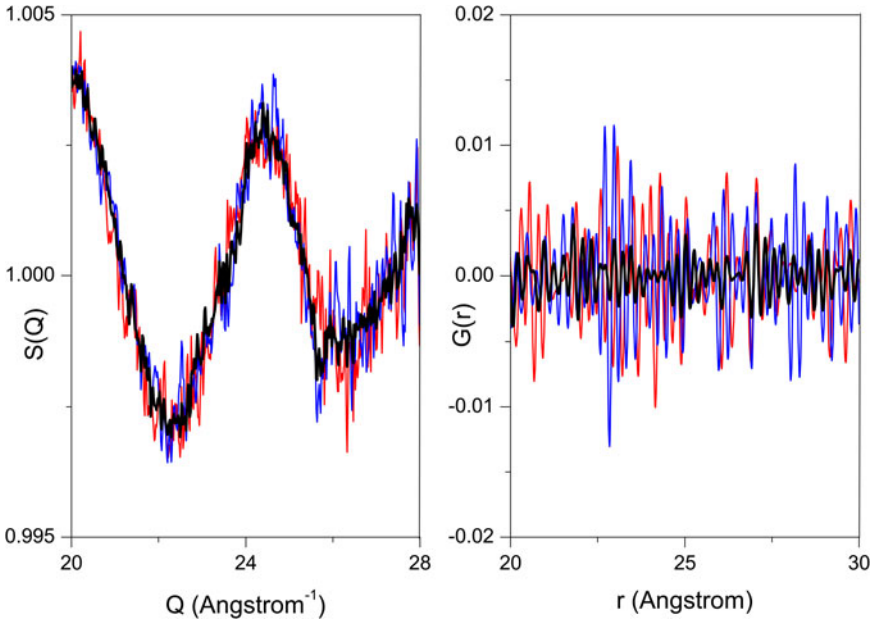

Figure 8. (Colour online) On the left side, the different noise in high Q in $S(Q)$ is displayed, whereas on the right, differences in the resultant $G(r)$ s are shown in the long range. The black line refers to an azimuthal range of 90°, averaging 20 images the red line refers to a reduced azimuthal range of 20°, averaging 20 images; whereas the blue line refers to an azimuthal range of 90°, considering one single image.

for Si–O distance, which is commonly located at 1.6 Å for these glasses (Bowron *et al.*, 2010) but is shifted to 1.65 if Q_{MAX} of 16 Å^{-1} is used.

Unlike for crystalline samples, the effect of statistics becomes more relevant in the case of glass samples. If Q_{MAX} is fixed at 28 Å^{-1}, $S(Q)$ is more noisy at high Q if a reduced azimuthal range is used or if only one single image is considered (see Figure 8, left side). This noise can affect the resultant $G(r)$s in the long range, generating amplified oscillations (red and blue curves), whereas in the short range the three curves are superimposable.

In consideration of that, the idea to increase Q_{MAX} (from 28 to 32 Å^{-1}) by reducing the azimuthal range (from 90° to 20°) must be evaluated as a function of the investigated sample and eventual presence of sample environment. Reducing the azimuthal range allows Q_{MAX} to be increased but also introduces noise and truncation at large distances in real space (r, as shown in Figure 8). In the present case, an increase of Q_{MAX} from 28 to 32 Å^{-1} does not significantly improve the resolution of atomic distances at low r.

A careful $S(Q)$ re-binning of the data might help to reduce some noise effects.

IV. CONCLUDING REMARKS

The effects of different Q ranges and statistics on the pair distribution function of different crystalline and glass samples have been investigated.

First of all, in order to obtain a PDF that is as accurate as possible, a careful preliminary data reduction is recommended, especially with the application of incident angle correction which may affect the raw intensity at high Q, where the diffuse scattering has a strong influence, and consequently the $G(r)$.

At these experimental conditions, putting the beam in the corner of the CCD was crucial, leading to cut-off Q_{MAX} value of at least 20 Å^{-1}, making in turn the $G(r)$ more accurate, both for crystalline and glass samples.

Counting statistics effect depend on the nature of the sample: for crystalline samples it does not lead to $G(r)$ peak broadening, whereas in the case of glass samples noise is more evident on the long range, enhancing the amplitude of oscillations.

ACKNOWLEDGEMENTS

Authors thank Gavin Vaughan (European Synchrotron Radiation Facility) and Monica Dapiaggi (University of Milan) for helpful discussions, and Giovanni Agostini (European Synchrotron Radiation Facility) for Zn-Edge EXAFS measurements at the BM23 beamline, whose results will be more in details described in a future work.

Billinge, S. J. L. (**2009**). "Local structure from total scattering and atomic pair distribution function (PDF) analysis," in *Powder Diffraction: Theory and Practice*, edited by R. E. Dinnebier and S. J. L. Billinge (The Royal Society of Chemistry, Cambridge), Chapter 16, pp. 464–493.

Bowron, D. T., Soper, A. K., Jones, K., Ansell, S., Birch, S., Norris, J., Perrott, D., Riedel, D., Rhodes, N. J., Wakefield, S. R., Botti, A., Ricci, M. A., Grazzi, F., and Zoppi, M. (**2010**). "NIMROD: the near and intermediate range order diffractometer of the ISIS second target station," Rev. Sci. Instrum. **81**, 033905.

Cassingham, N. J., Stennet, M. C., Bingham, P. A., Hyatt, N. C., and Aquilanti, G. (**2011**). "The structural role of Zn in nuclear waste glasses," Int. J. Appl. Glass Sci. **2**(4), 343–353.

Farrow, C. L., Juhas, P., Liu, J. W., Bryndin, D., Bozin, E. S., Bloch, J., Proffen, Th., and Billinge, S. J. L. (**2009**). "PDFfit2 and PDFgui: computer programs for studying nanostructure in crystals," J. Phys. Condens. Matter **19**, 335219.

Hammersley, A. P., Svensson, S. O., Hanfland, M., Fitch, A. N., and Hausermann, D. (**1996**). "Two-dimensional detector software: from real detector to idealized image or two-theta scan," High Press. Res. **14**, 235–248.

Hong, X., Chen, Z., and Duffy, T. S. (**2012**). "Absolute x-ray energy calibration over a wide energy range using a diffraction-based iterative method," Rev. Sci. Instrum. **83**, 063901.

Kahn, R., and Fourme, R. (**1982**). "Macromolecular crystallography and polarization correction," J. Appl. Crystallogr. **15**, 330–337.

Juhas, P., Davis, T., Farrow, C. L., and Billinge, S. J. L. (**2013**). "PDFgetX3: a rapid and highly automatable program for processing powder diffraction

https://doi.org/10.1017/S0885715614001304 Published online by Cambridge University Press

data into total scattering pair distribution functions," J. Appl. Crystallogr. **46**, 560–566.

Labiche, J. C., Mathon, O., Pascarelli, S., Newton, M. A., Ferre, G. G., Curfs, C., Vaughan, G., Homs, A., and Carreira, D. F. (**2007**). "Invited article: the fast readout low noise camera as a versatile x-ray detector for time resolved dispersive extended x-ray absorption fine structure and diffraction studies of dynamic problems in materials science, chemistry, and catalysis," Rev. Sci. Instrum. **78**, 091301.

Masadeh, A. S., Bozin, E. S., Farrow, C. L., Paglia, G., Juhas, P., Billinge, S. J. L, Karkamkar, A., and Kanatzidis, M. G. (**2007**). "Quantitative size-dependent structure and strain determination of CdSe nanoparticles using atomic pair distribution function analysis," Phys. Rev. B **76**, 115413.

Ponchut, C. (**2006**). "Characterization of X-ray area detectors for synchrotron beamlines," J. Synchrotron Radiat. **13**, 195–203.

Wu, G., Rodrigues, B. L., and Coppens, P. (**2002**). "The correction of reflection intensities for incomplete absorption of high-energy X-rays in the CCD phosphor," J. Appl. Crystallogr. **35**, 356–359.

Wyckoff, R. W. G. (**1963**). American Mineralogist Crystal Structure Database.

Xu, Y. N. and Ching, W. Y. (**1993**). American Mineralogist Crystal Structure Database.

https://doi.org/10.1017/S0885715614001304 Published online by Cambridge University Press